

# Optical Rectification in 4H-SiC: Paving the Way to Generate Strong Terahertz Field with Ultra-Wide Bandwidth

Fangjie Li<sup>1,2</sup>, Kai Zhong<sup>1,2\*</sup>, Yiwen Zhang<sup>1,2</sup>, Tong Wu<sup>3</sup>, Yuxin Liu<sup>1,2</sup>, Hongzhan Qiao<sup>1,2</sup>, Jining Li<sup>1,2</sup>, Degang Xu<sup>1,2</sup>, and Jianquan Yao<sup>1,2</sup>

<sup>1</sup> *School of Precision Instruments and Optoelectronics Engineering, Tianjin University, Tianjin, China*

<sup>2</sup> *Key laboratory of Opto-electronic Information Technology, Ministry of Education (Tianjin University), Tianjin, China*

<sup>3</sup> *School of Marine Science and Technology, Tianjin University, Tianjin, China*

**Abstract** The 4H-SiC crystal is found to have great potential in terahertz generation via nonlinear optical frequency conversion due to extremely high optical damage threshold, wide transparent range, etc. In this paper, optical rectification (OR) with tilted-pulse-front (TPF) setting based on 4H-SiC crystal is proposed. The theory accounts for the optimization of incident pulse pre-chirping on the TPF OR process under high-intensity femtosecond (fs) laser pumping. Compared with the currently recognized LiNbO<sub>3</sub>-based TPF OR which generates single-cycle terahertz pulse within 3 THz, 4H-SiC demonstrates significant advantage in producing ultra-widely tunable (up to over 14 THz, TPF angle 31°-38°) terahertz waves with high efficiency ( $\sim 10^{-2}$ ) and strong field ( $\sim \text{MV/cm}$ ). Besides, the spectrum characteristics, as well as the evolution from single- to multi-cycle terahertz pulses

This peer-reviewed article has been accepted for publication but not yet copyedited or typeset, and so may be subject to change during the production process. The article is considered published and may be cited using its DOI.

This is an Open Access article, distributed under the terms of the Creative Commons Attribution licence (<https://creativecommons.org/licenses/by/4.0/>), which permits unrestricted re-use, distribution, and reproduction in any medium, provided the original work is properly cited.

10.1017/hpl.2023.52

can be modulated flexibly by pre-chirping. The simulation results show that 4H-SiC enables terahertz frequency extending to an unprecedented range by OR, which has extremely important potential in strong-field terahertz applications.

*Key words: Optical rectification; silicon carbide; terahertz radiation; tilted-pulse-front*

---

\*Correspondence to: Kai Zhong, School of Precision Instruments and Optoelectronics Engineering, Tianjin University, Tianjin 300072, China. Email: zhongkai@tju.edu.cn

## I. INTRODUCTION

Strong-field terahertz sources have played important roles in nonlinear terahertz spectroscopy<sup>[1-3]</sup>, strong-field terahertz physics<sup>[4,5]</sup>, electron manipulation<sup>[6]</sup>, particle acceleration<sup>[7]</sup>, etc. There are a few available technologies that permit powerful terahertz generation, such as the free electron laser (FEL)<sup>[8,9]</sup>, photoconductive antenna (PCA)<sup>[10-13]</sup>, spintronic terahertz emitter (STE)<sup>[14,15]</sup>, laser-plasma interaction<sup>[16,17]</sup>, and optical rectification (OR)<sup>[18-21]</sup>. The FEL can produce strong terahertz field with peak amplitude up to dozens of MV/cm, but accompanied by obvious shortcomings of huge volume, high complexity and unacceptable cost. The PCA suffers from limited damage threshold so that the terahertz field is relatively low even if a large-aperture PCA is used<sup>[13]</sup>. The plasma excited by high-intensity femtosecond laser pulses emits ultra-broadband coherent radiation spanning from X-ray to terahertz waves and the terahertz field can be further enhanced by two-color filamentation<sup>[16,17]</sup>. Due to its highly nonlinear and phase-sensitive nature in laser-gas interaction, the stability is a major problem<sup>[22]</sup>. Based on spintronics in ferromagnetic/non-magnetic heterostructure, the STE is promising for terahertz generation with wide frequency band, low cost and high field intensity<sup>[15]</sup>. It has attracted much attention in recent years and its

significance in ultra-broadband measurements, magnetic structure imaging and near-field microscopy has been recognized. However, there is obstacle for STE to produce multi-cycle terahertz pulses and the technological maturity is still a problem for applications at the present stage. Generally, OR, which originates from second-order nonlinear optical (NLO) effects induced by ultrashort laser pulses, is believed to be the most effective and practical technology to obtain table-top terahertz sources with high efficiency close to or even beyond the Manley-Rowe limit. The major concerns of OR include the physical and optical properties of the NLO crystal, as well as the feasibility of realizing the phase-matching (PM) condition.

Semiconductor crystals such as ZnTe and GaP have reasonable transmission in the terahertz range and PM can be fulfilled at suitable pump wavelength, e.g., ZnTe pumped by Ti:sapphire lasers around 800 nm and GaP pumped by Yb-doped lasers around 1030 nm<sup>[23-25]</sup>. Low laser-induced damage threshold (LIDT) and high two-photon absorption (2PA) due to narrow bandgap are the primary defects of these semiconductors<sup>[26,27]</sup>, which severely limits the conversion efficiency and maximum terahertz pulse energy<sup>[22]</sup>. Organic crystals possess extremely high nonlinearity and can produce strong terahertz pulses within one coherent length, represented by DAST and BNA<sup>[18,19]</sup>, but they are usually excluded by robust systems because of deliquescence, low LIDT and serious terahertz absorption<sup>[22]</sup>. As a popular crystalline material in nonlinear optics, lithium niobate (LiNbO<sub>3</sub>) has wide bandgap, high nonlinear coefficient and LIDT<sup>[28,29]</sup>, enabling widely tunable terahertz generation via stimulated polariton scattering<sup>[29-31]</sup>. However, LiNbO<sub>3</sub>-based OR used to be unachievable for a long time due to the difficulty in PM<sup>[22]</sup>, until the tilted-pulse-front (TPF) technique was proposed.

The TPF technique was first introduced into OR in 2002<sup>[32]</sup>. Since then, TPF OR has been extensively studied, mainly focusing on LiNbO<sub>3</sub> and some cubic semiconductors<sup>[20,21,33-50]</sup>. The

special significance of TPF is that it greatly lowers the rigorous requirement for PM condition in OR. TPF allows pumping at longer wavelength to reduce free-carrier absorption (FCA) which is mainly caused by 2PA and can improve the OR efficiency in cubic semiconductors such as ZnTe and GaAs<sup>[21,49,50]</sup>. Moreover, PM for LiNbO<sub>3</sub> OR pumped by intense femtosecond lasers can be realized for efficient strong-field terahertz generation at a typical TPF angle around 63°<sup>[20,33-37]</sup>. Quite a few theoretical models have been developed to explain and optimize this technique<sup>[38-48]</sup>. The maximum single-pulse energy has reached the milestone mJ-level recently<sup>[20]</sup>, which is of great significance to motivate extreme terahertz applications. However, only the low-frequency region below 3.5 THz can be generated via TPF OR in LiNbO<sub>3</sub>. Limited by the sharp increase of absorption coefficient due to phonon vibrations<sup>[51,52]</sup>, extending the terahertz spectrum to the high-frequency part in LiNbO<sub>3</sub> is extremely difficult. In addition, large TPF angle in LiNbO<sub>3</sub> causes serious beam distortion<sup>[21,37,38,49]</sup> and group velocity dispersion due to angular dispersion (GVD-AD)<sup>[43,44]</sup>, which prevents maintaining PM condition in the cascaded DFG process.

Filling up the nonexistent high-frequency terahertz spectrum has always been desired but impossible by TPF OR in LiNbO<sub>3</sub>, until we focused on the crystalline silicon carbide (SiC), a representative wide-bandgap semiconductor material. SiC has more than 200 polymorphs, among which the positive uniaxial 4H-SiC crystal (6mm group point) is the most promising one in nonlinear optics. 4H-SiC has ultra-high LIDT (up to 80 GW/cm<sup>2</sup> with 10 ns laser pulse at 1064 nm<sup>[53]</sup>), wideband transparency (0.37-5.6 μm and 0.1-18 THz<sup>[54-58]</sup>) and large bandgap (3.26 eV<sup>[59]</sup>) compared with all the other available second-order nonlinear crystals for terahertz generation. Its excellent optical properties guarantee intense optical pumping under powerful Ti:sapphire amplifiers<sup>[58]</sup> to generate strong-field and broadband terahertz radiation. There have been a few reports to explore the potential of SiC crystals in terahertz generation via NLO effects in recent

years. Strait et al. demonstrated coherent terahertz radiation produced by OR in a 6H-SiC wafer for the first time<sup>[60]</sup>. Naftaly et al. measured the transparency and birefringence of 4H-SiC in the range of 0.1-20 THz, and predicted broadband terahertz generation up to 18 THz by DFG<sup>[57]</sup>. Fischer et al. achieved tunable transient DFG terahertz source between 5 and 15 THz using 4H-SiC pumped by two femtosecond lasers, and the electro-optic detection based on 4H-SiC as well<sup>[58]</sup>. However, simultaneous generation of broadband terahertz spectrum in 4H-SiC covering the transparent range has been impossible due to the challenge in fulfilling the PM condition. In addition, the high LIDT of this material has not been fully used which greatly limits the conversion efficiency. Once an extremely strong pump field is applied, an essential condition to ensure high OR efficiency in 4H-SiC, the self-phase modulation (SPM) and FCA effects would become critical in the nonlinear process.

Considering the bright prospect of 4H-SiC in strong-field broadband terahertz generation by OR, the TPF technique is introduced under intense laser pumping in this paper. Compared with LiNbO<sub>3</sub>, the TPF angle required for 4H-SiC is much smaller, which reduces the GVD-AD and beam distortion, increases the effective interaction length and uniformity in terahertz generation, and favors one-dimensional (1D) spatial model analysis to simulate the dynamics based on the 4<sup>th</sup> Runge-Kutta method. The accuracy of the model was assured by simultaneous consideration of the following factors: (i) NLO coupled interaction of the terahertz and optical waves, reflected in the resonant cascading effects including cascaded DFG and sum frequency generation (SFG); (ii) angular dispersion (AD) and material dispersion (MD); (iii) linear absorption and FCA at terahertz frequency caused by three-photon absorption (3PA); (iv) SPM; (v) pre-chirping of the input pump pulses. On this basis, the evolution of terahertz and optical waves were analyzed quantitatively. Ultimately, ultra-widely tunable (up to over 14 THz), high-efficiency ( $\sim 10^{-2}$ ) and strong-field

(MV/cm) terahertz generation was predicted by illuminating well-chirped ultrashort (30 fs) laser pulses at 800 nm to 4H-SiC crystals. It was shown that single- and multi-cycle terahertz pulses can be modulated by pre-chirping and the central frequency of the terahertz spectrum is tunable by varying the TPF angle. The results indicate that 4H-SiC enables the terahertz frequency extending to an unprecedented range by OR, which has extremely important potential in strong-field terahertz applications.

## II. THEORETICAL MODEL

Matching between the group velocity of ultrashort optical pulses and the phase velocity of terahertz waves determines the OR efficiency, where the main influence factors include pump wavelength, polarization, and crystal orientation. TPF gives another freedom, the TPF angle  $\gamma$ , to fulfill the matching condition with variable optical wavelength and terahertz frequency. The requirement of  $\gamma$  is calculated by  $\cos\gamma = n_g/n_{\text{THz}}$ <sup>[32]</sup>, where  $n_g$  and  $n_{\text{THz}}$  are the group refractive index of the optical pulse and phase refractive index of terahertz waves, respectively. Based on the Sellmeier equations of 4H-SiC<sup>[55,58]</sup>, the typical TPF angle of  $\gamma=32^\circ$  is obtained by substituting  $n_g=2.7610$  ( $\lambda_{\text{op}} = 800$  nm) and  $n_{\text{THz}}=3.2445$  ( $\lambda_{\text{THz}} = 60 \mu\text{m}$ ) for e-e $\rightarrow$ e PM condition. Such a TPF angle is half of that in LiNbO<sub>3</sub>, which highly benefits the TPF OR process. In addition to increasing effective interaction length, improving spatial uniformity and alleviating distortion, smaller TPF angle also promise better simulation accuracy. A variety of theoretical models have been developed so far<sup>[38-48]</sup>, basically including 1D to 3D spatial models with/without considering the cascading effects, among which the 1D model with cascading effects is believed most fits the situation here. On one hand, the 1D model greatly simplifies complexity while ensuring the accuracy in case of small TPF angle. On the other hand, the spectral re-shaping of the optical pump pulse via cascading effects requires consideration, otherwise, the conversion efficiency will be overestimated. Finally, when

illuminated by strong laser pulses, complex nonlinear processes including SPM and photon absorption induced FCA of terahertz waves, cannot be neglected. The 1D coupled wave equations of TPF OR with cascading, SPM and FCA effects are given by<sup>[35,39]</sup>

$$\frac{dA_{THz}(\Omega, z)}{dz} = -\frac{\alpha_{THz}(\Omega)}{2} A_{THz}(\Omega, z) - \frac{j\Omega^2}{2c^2 k(\Omega)} \chi_{eff}^{(2)} \int_0^\infty A_{op}(\omega + \Omega, z) A_{op}^*(\omega, z) \exp\{-j[k(\omega + \Omega) - k(\omega) - k(\Omega)]z\} d\omega, \quad (1a)$$

$$\begin{aligned} \frac{dA_{op}(\omega, z)}{dz} = & -\frac{\alpha_{op}(\omega)}{2} A_{op}(\omega, z) - \frac{j\omega^2}{2c^2 k(\omega)} \chi_{eff}^{(2)} \left\{ \int_0^\infty A_{op}(\omega + \Omega, z) A_{THz}^*(\Omega, z) \exp\{-j[k(\omega + \Omega) - k(\omega) - k(\Omega)]z\} + \right. \\ & \left. \int_0^\infty A_{op}(\omega - \Omega, z) A_{THz}(\Omega, z) \exp\{-j[k(\omega - \Omega) - k(\omega) + k(\Omega)]z\} \right\} d\Omega \\ & - Ft \left\{ j \frac{\varepsilon_0 \omega_0 n(\omega_0) n_2(z)}{2} |A_{op}(z, t)|^2 A_{op}(z, t) \right\}, \end{aligned} \quad (1b)$$

and the wave numbers of the terahertz and optical fields are

$$k(\Omega) = \frac{n(\Omega)\Omega}{c}, \quad (2a)$$

$$k(\omega) = \frac{1}{\cos \gamma} \frac{n(\omega)\omega}{c} - \frac{(\omega - \omega_0)^2}{2} \frac{n_g^2(\omega_0)}{\omega_0 c n(\omega_0)} \tan^2 \gamma, \quad (2b)$$

respectively, where  $\omega$  and  $\Omega$  represent the angular frequencies of the optical and terahertz waves,  $A_{op}$  and  $A_{THz}$  are the envelopes of the optical and terahertz fields,  $\alpha_{op}$  and  $\alpha_{THz}$  are the absorptions in optical and terahertz regions,  $c$  is the speed of light in the vacuum,  $\chi_{eff}^{(2)}$  is the effective second-order nonlinear susceptibility,  $\varepsilon_0$  is the vacuum permittivity,  $\omega_0$  is the central optical angular frequency, and  $n$  and  $n_2$  are the refractive index and nonlinear refractive index<sup>[55,58,61]</sup>, respectively.

Equation (1a) describes terahertz generation by DFG between different optical frequency components, while the Equation (1b) indicates the DFG and SFG processes between optical and terahertz frequencies. The last term of the Equation (1b) shows the SPM effect, which would widen the optical spectrum significantly under intense pumping, resulting in decrease of pump spectral intensities and hindering terahertz generation seriously. The spectral widening caused by stimulated Raman scattering (SRS) was ignored because the major Raman peak of 4H-SiC locates at around 23 THz, beyond the bandwidth of typical Ti:sapphire laser pulses with Fourier-transform-limited (FTL) duration of 30 fs<sup>[62]</sup>. The second term of the Equation (2b) corresponds to GVD due to AD, which deteriorates the PM condition with red shifting the pump spectrum.

The SPM effect can be relieved effectively via pre-chirping before injecting the pump beam because of the reduction of pump intensity due to pulse broadening. Given the Gaussian envelope of the electric field is  $A(t)$ , its frequency-domain expression after chirping is

$$A(\omega) = \text{Ft}\{A(t)\} \exp\{-j\phi(\omega)\}, \quad (3a)$$

where  $\phi(\omega)$  is the frequency-dependent additional phase, given by

$$\phi(\omega) = \frac{GDD}{2}(\omega - \omega_0)^2 + \frac{TOD}{6}(\omega - \omega_0)^3, \quad (3b)$$

where GDD and TOD are the group delay dispersion and third order dispersion, respectively.  $\phi(\omega)$  leads to the broadening of pulse duration and further affects the PM condition as shown in the Equation (1).

Unlike the photogenerated carriers in the photo-dember effect which help screen the doping-induced interfacial electric field and generate terahertz radiation in the form of the time derivative of the net current<sup>[63, 64]</sup>, the photogenerated carriers in OR tend to exhibit absorption of



photons. Under intense pumping, the increase of free-carrier density caused by photon absorption leads to serious FCA effect, thus the absorption is increased to  $\alpha_{\text{THz}} + \alpha_{\text{fc}}$  instead of the original  $\alpha_{\text{THz}}$  in the Equation (1)<sup>[65]</sup>. The density of free carrier  $N_{\text{fc}}$  is given by<sup>[65]</sup>

$$N_{\text{fc}} = \frac{IT_z}{hc / \lambda_0} \left( \alpha_1 + \frac{1}{2} \alpha_2 I + \frac{1}{3} \alpha_3 I^2 + \dots \right), \quad (4)$$

where  $I$  is the time-averaged pump pulse intensity over the pulse duration,  $\lambda_0$  is the central pump wavelength, and  $\alpha_1$ ,  $\alpha_2$  and  $\alpha_3$  are the linear, two-photon, and three-photon absorption coefficients, respectively. Only 3PA is considered because of the large band gap of 4H-SiC<sup>[61]</sup>.  $T_z$  is the pump pulse duration in the crystal that may vary with propagation distance due to dispersion, called pulse-stretching effect<sup>[38]</sup>.  $T_z$  is regarded as a constant here since pulse-stretching in 4H-SiC can be relieved by pre-chirping the pump laser pulse<sup>[65]</sup>. The FCA cross section  $\sigma$  is assumed to be  $5 \times 10^{-18} \text{ cm}^2$ <sup>[66]</sup> thus the pump absorption could be estimated by the saturated 3PA model<sup>[67]</sup> under intense pumping, where pre-chirping is also proved effective to reduce the pump absorption until negligible. Since the pump pulse duration  $T_z$  and intensity  $I$  are both unchanged under pre-chirping, the free-carrier density  $N_{\text{fc}}$  in the crystal is also regarded as invariant along the pump direction. However, compared with the pump absorption, the terahertz absorption is much more serious even if pre-chirping is present. Therefore, the terahertz absorption by free carriers  $\alpha_{\text{fc}}$  must be considered, which is calculated by the Drude model:

$$\alpha_{\text{fc}} = \frac{2\Omega}{c} \text{Im} \left\{ \sqrt{\varepsilon_{\infty} \left( 1 - \frac{\omega_p^2}{\Omega^2 + i\Omega / \tau_{sc}} \right)} \right\}, \quad (5)$$

where  $\epsilon_\infty$  is the high-frequency dielectric constant,  $\tau_{sc}$  is the electron scattering time,  $\omega_p = e\sqrt{N_{fc} / \epsilon_0 \epsilon_\infty m_{eff}}$  is the plasma frequency,  $e$  is the electron charge, and  $m_{eff}$  is the electron effective mass.

### III. RESULTS AND ANALYSIS

#### TPF OR without Pre-chirping

In order to compare the performance of TPF OR in LiNbO<sub>3</sub> and 4H-SiC, the terahertz output and pump evolution in LiNbO<sub>3</sub> (at 100 K) and 4H-SiC (room temperature) were studied and shown in Figure 1, respectively, both in the absence of pre-chirping. The difference between two crystals can be observed from the same low pump intensity at 50 GW/cm<sup>2</sup>, where the serious SPM and FCA effects are reflected by high-intensity pumping at 500 GW/cm<sup>2</sup> in 4H-SiC. The FTL pump pulse durations corresponding to LiNbO<sub>3</sub> and 4H-SiC were 350 fs and 30 fs, respectively, the former of which was a recognized value for LiNbO<sub>3</sub><sup>[38]</sup> and the later was designated for high-frequency terahertz generation with mature ultrafast Ti:Sapphire amplifiers. For comparison, the LiNbO<sub>3</sub> crystal pumping at the FTL pulse duration of 30 fs was also studied. The other parameters are given in Table I, where those in brackets represent the input of LiNbO<sub>3</sub>. Note that the  $\chi_{eff}^{(2)}$  of 4H-SiC was calculated via Miller's rule<sup>[68]</sup> by considering  $d_{33}=11.7$  pm/V for second harmonic generation at 1064 nm<sup>[69]</sup>. The linear absorption coefficients of 4H-SiC in optical and terahertz regions were both ignored.

**Table I**

Input parameters for analyzing TPF OR in LiNbO<sub>3</sub> and 4H-SiC crystals.

Parameter	Value
Central pump wavelength $\lambda_0$	800 nm
FTL duration $\tau_0$	30 fs (30 fs, 350 fs)

TPF angle $\gamma$	$32^\circ$ (61.64°)
Nonlinear refractive index $n_2$	$10^{-19}$ m <sup>2</sup> /W
Nonlinear susceptibility $\chi_{\text{eff}}^{(2)}$	37.6 pm/V (360 pm/V)
Absorption coefficient $\alpha$	0 (6 cm <sup>-1</sup> )
GDD	0 fs <sup>2</sup>
Peak intensity $I_{\text{op}}$	50 GW/cm <sup>2</sup> & 500 GW/cm <sup>2</sup>

---

According to Figure 1(a), the maximum OR efficiencies are 0.10% (at 0.60 mm), 2.18% (at 1.38 mm), 0.27% (at 1.44 mm) and 0.07% (at 0.19 mm) under the condition of LiNbO<sub>3</sub> pumped by 30 fs and 350 fs pulses at 50 GW/cm<sup>2</sup>, 4H-SiC pumped by 30 fs pulses at 50 GW/cm<sup>2</sup> and 500 GW/cm<sup>2</sup>, respectively. The high efficiency of LiNbO<sub>3</sub> pumped at 350 fs originates from the strong spectral intensity and large nonlinear susceptibility. While pumping at 30 fs, the efficiency is low because narrower FTL pulse duration corresponds to wider spectrum, which leads to lower spectral intensity and spectral waste out of the PM bandwidth. The efficiency decline with LiNbO<sub>3</sub> after the maximum point are mainly caused by linear absorption and back conversion, which can be observed from Figure 1(c) that shorter pump wavelengths are produced through SFG. As to 4H-SiC, the OR efficiency is extremely low with small propagation distance  $L$  (hundred- $\mu$ m level) even if the pump intensity is as high as 500 GW/cm<sup>2</sup>, because serious SPM and FCA effects limit the cascading effect and lead to strong terahertz absorption. Despite of low efficiency, the obvious advantage of 4H-SiC over LiNbO<sub>3</sub> is apparent, that is, the capability to generate wide terahertz spectrum benefitting from its flat dispersion curve in the terahertz range. Figure 1(b) shows the spectrum obtained at the optimal  $L$ . The terahertz frequency is extended to over 12 THz with the 4H-SiC crystal, much wider than LiNbO<sub>3</sub> limiting to below 3 THz. A shorter 4H-SiC crystal would produce even wider spectrum but the frequencies below 5 THz are strongly absorbed by the FCA effect in case of high-intensity pumping. Furthermore, the widening and red shift of the pump

spectrum in 4H-SiC caused by the cascading effect is not apparent, as shown in Figure 1(d), but SPM dominates, which also leads to the decline of terahertz intensity shown in Figure 1(b). Besides, larger red shift in Figure 1(d) implies higher conversion efficiency in Figure 1(a), even if under low-intensity pumping. Compared with 4H-SiC, the efficient cascading effect in LiNbO<sub>3</sub> pumped at 350 fs results in remarkable spectrum widening and red shift, while SPM can be ignored<sup>[43]</sup>. On the contrary, the spectrum widening and red shift are both inconspicuous in LiNbO<sub>3</sub> pumped at 30 fs, which can be explained by the low efficiency and short propagation distance. Another fact that requires consideration is the effective interaction length, which is related to dispersion, TPF angle and FTL pulse duration, etc. It will intrinsically decrease using ultrashort FTL pulse duration due to the dispersion in NLO crystals<sup>[38]</sup>. Pre-chirping the incident pump pulse is an effective way to increase effective interaction length.

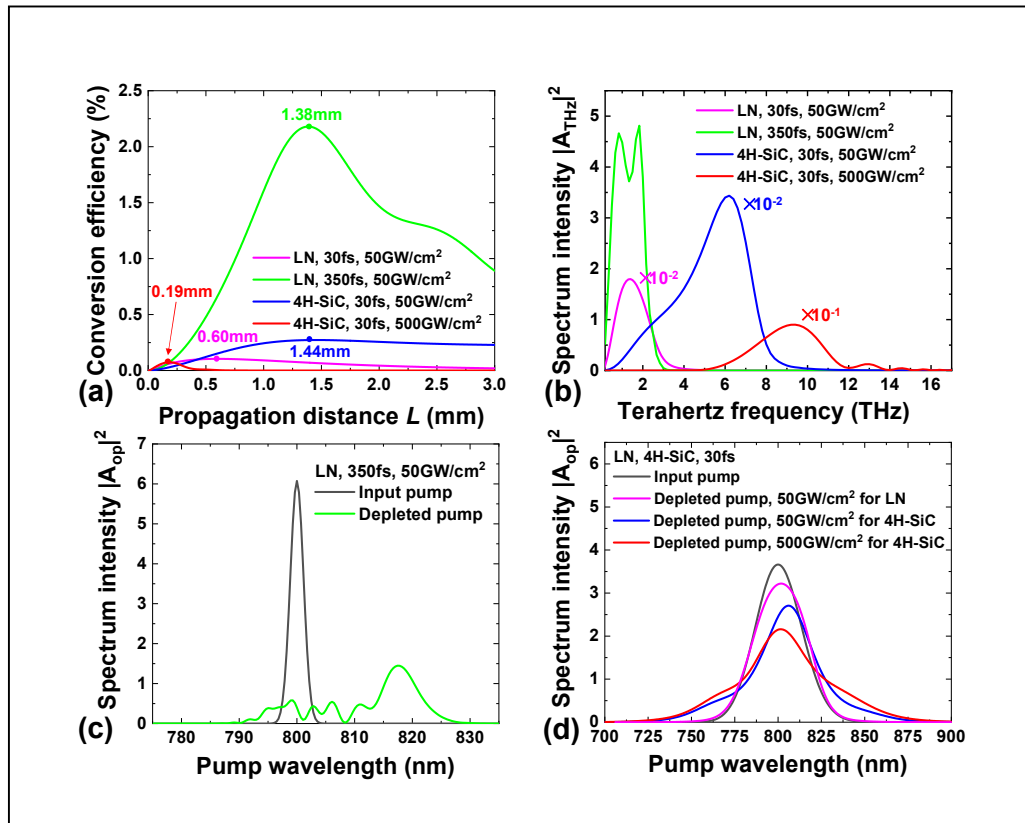


**Figure 1.** Comparison of terahertz output and pump evolution in LiNbO<sub>3</sub> and 4H-SiC crystals without pre-chirping. (a) Conversion efficiencies of terahertz generation versus propagation distance  $L$  along the  $z$  direction. (b) Terahertz spectrums  $|A_{\text{THz}}|^2$  in linear scale at the optimal  $L$  in (a), multiplied by 1,  $10^{-2}$  and  $10^{-1}$ , respectively. (c) and (d) depict the corresponding pump evolution processes influenced by cascading and SPM effects, including depletion, widening and frequency shift compared with the input pump. In (d), low- and high-intensity input pumps are normalized to distinguish their difference more clearly.

### TPF OR in 4H-SiC with Pre-chirping

Strong SPM and FCA effects seriously limit terahertz generation under intense pumping, so that coherent terahertz radiation can only be generated in thin 4H-SiC wafers with poor efficiency. Pre-chirping the pump pulse provides an effective solution to improve the OR efficiency with at least the following advantages: (a) relieving spectrum widening originated from SPM; (b) reducing pump and terahertz absorption caused by FCA; (c) increasing effective interaction length; (d) lowering the risk of damage to the 4H-SiC crystal and other optical elements; (e) modulating the terahertz spectrum and temporal waveform, etc. A comprehensive 1D model has been developed considering the pre-chirping of the incident pump pulse, which can be realized by adding variable GDD through the acousto-optic programmable dispersion filter. The peak pump intensity is  $I_{\text{op}}=500 \text{ GW/cm}^2$  before pre-chirping, while the other parameters are given in Table I. Six typical TPF angles ( $31^\circ$ ,  $31.5^\circ$ ,  $32^\circ$ ,  $33^\circ$ ,  $35^\circ$  and  $38^\circ$ ) were simulated and analyzed with the 2D plots of OR efficiency shown in Figure 2.

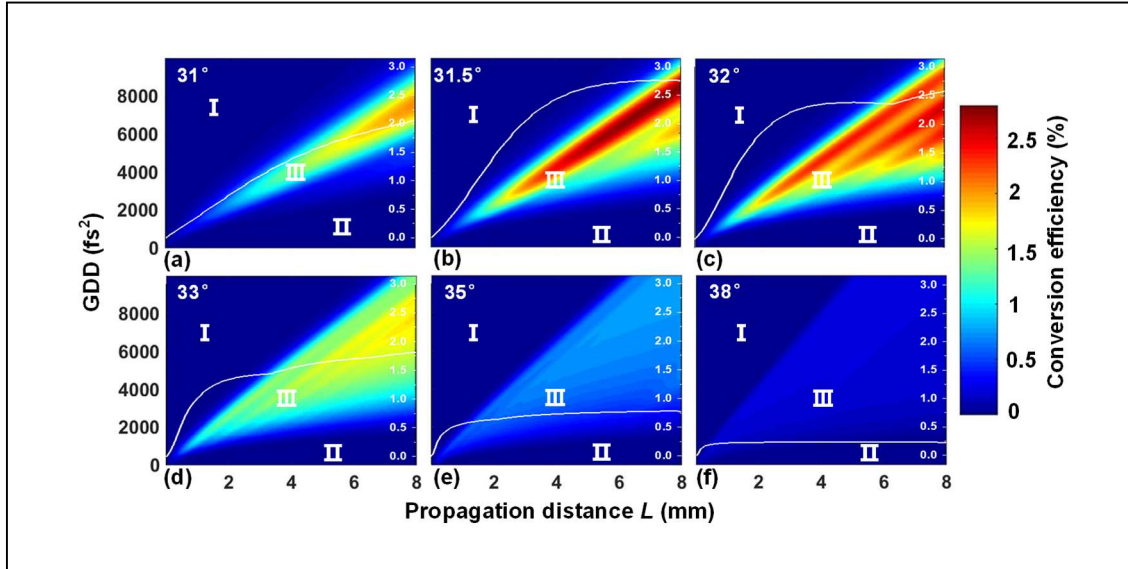


**Figure 2.** TPF OR conversion efficiency (color scale) along the propagation distance  $L$  for various GDD values at six TPF angles from  $31^\circ$  to  $38^\circ$ . The white curves represent the maximum efficiency ( $\eta_{\max}$ ) obtained by optimizing the GDD at each  $L$ . Area I, II and III indicate different OR efficiencies affected by GDD, defined as excessive, insufficient and suitable pre-chirping, respectively.

Clearly, the OR efficiency is significantly improved by pre-chirping the pump pulse. The linear increase of optimal GDD with  $L$  brings a benefit that dispersion-induced pulse stretching is greatly weakened, which is consistent with the assumption of constant pulse duration through the crystal. Tuning the TPF angle from  $31^\circ$  to  $38^\circ$  allows the generation of higher terahertz frequency (which will be described later), accompanied by requiring more GDD at a certain  $L$ . Meanwhile, the  $\eta_{\max}$  curve becomes easier to saturate, gradually decreasing from  $>2\%$  (TPF angle  $31^\circ$ ) to  $0.23\%$  (TPF angle  $38^\circ$ ). In order to reveal the physical process, each 2D efficiency distribution plot can be divided into three areas:

Area I, excessive pre-chirping. Pre-chirping the pump pulse results in the change of pump spectral phase  $\phi(\omega)$ , so that inducing phase mismatch reflected in the Equation (1), and the OR efficiency is extremely low.

Area II, insufficient pre-chirping. SPM and FCA dominate and affect the OR efficiency. the former causes spectral widening while the latter leads to strong terahertz absorption, especially at the low-frequency range. Therefore, this area (low efficiency) is larger at smaller TPF angles.

Area III, suitable pre-chirping. The OR efficiency increases with  $L$  until saturation. Obvious efficiency oscillations can be noticed at TPF angles from  $31.5^\circ$  to  $33^\circ$  after the saturation of  $\eta_{\max}$ . More GDD and larger TPF angle tends to generate more and denser oscillations. The oscillation characteristics are related to the terahertz spectrum splitting, widening and absorption, which will be explained later from the spectral evolution.

In order to study the influence of pre-chirping on terahertz generation and optimize the pump parameters, the 2D plots of terahertz spectrum intensity  $|A_{\text{THz}}|^2$  versus GDD at six TPF angles are calculated and shown in Figure 3. Benefiting from the flat dispersion and high transparency of 4H-SiC in the whole terahertz band, widely tunable terahertz spectrum can be achieved by precisely varying the TPF angle and pre-chirping. Here the optimal condition is defined as the values of GDD and  $L$  that guarantee efficient generation of smooth and intensity-concentrated terahertz spectrum. It can be noticed that increasing the TPF angle shifts the terahertz spectrum towards higher frequency and shrinks the bandwidth, while the optimal GDD should be larger as well. Intense pump pulse with insufficient GDD would lead to spectral widening and terahertz absorption due to SPM and FCA effects, respectively. Particularly, in the low-frequency range, more spectrum splitting and widening emerge because of larger PM allowance together with higher absorption, resulting in declined efficiency and deterioration of the terahertz spectrum. On the

other hand, excessive GDD destroys the PM condition, so that the cascading effect cannot be delivered within the  $L$  of 4 mm, showing as a rapid decline in efficiency although SPM and FCA are both relatively weak. In this case, effective terahertz generation requires longer  $L$ , as shown in Figure 2. In general, with the increase of GDD, the terahertz spectrums experience splitting and widening with low efficiency, towards smooth and concentrated with high efficiency, and finally, decay rapidly due to the destruction of PM condition. Only when the optimal GDD is satisfied, that is,  $3900 \text{ fs}^2$ ,  $4200 \text{ fs}^2$ ,  $4500 \text{ fs}^2$ ,  $5050 \text{ fs}^2$ ,  $6000 \text{ fs}^2$  and  $7550 \text{ fs}^2$  for the six TPF angles, respectively, can high-quality terahertz spectrum be generated. Figure 3 shows the evolution and basic parameters to modulate of terahertz spectrum by pre-chirping the pump pulse.

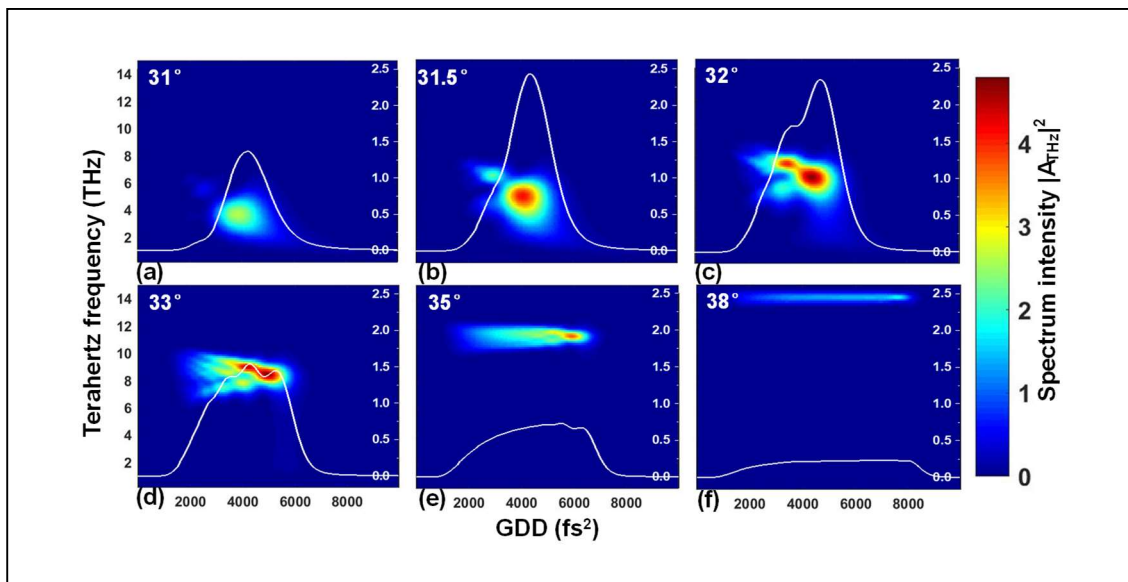


**Figure 3.** Terahertz spectrum intensity  $|A_{\text{THz}}|^2$  (color scale) as a function of GDD at six TPF angles from  $31^\circ$  (a) to  $38^\circ$  (f), when  $L=4$  mm. The white curves indicate the conversion efficiency regulated by GDD.

An intuitional demonstration of the widely tunable and smooth terahertz spectrum is shown in Figure 4, where optimal pre-chirping is applied and all the terahertz spectrums are in linear scale.



Basically, the higher central terahertz frequency, the narrower spectrum, e.g., the 3-dB spectral ranges are 2.40-4.83 THz, 3.29-6.14 THz, 5.24-7.29 THz, 7.71-9.05 THz, 10.86-11.64 THz and 13.83-14.33 THz for the TPF angles at  $31^\circ$ ,  $31.5^\circ$ ,  $32^\circ$ ,  $33^\circ$ ,  $35^\circ$  and  $38^\circ$ , respectively. The bandwidth of TPF angle at  $31^\circ$  is narrower than that at  $31.5^\circ$  because the FCA effect has stronger absorption to low terahertz frequencies. The FCA effect also contributes to shifting the terahertz spectrum towards the high-frequency part, as shown in Figure 4(b). The simulation results of peak frequency using the 1D model deviate more at low frequencies, which is another proof that the FCA effect has restrictions on the terahertz spectral intensity and overall efficiency in this range.

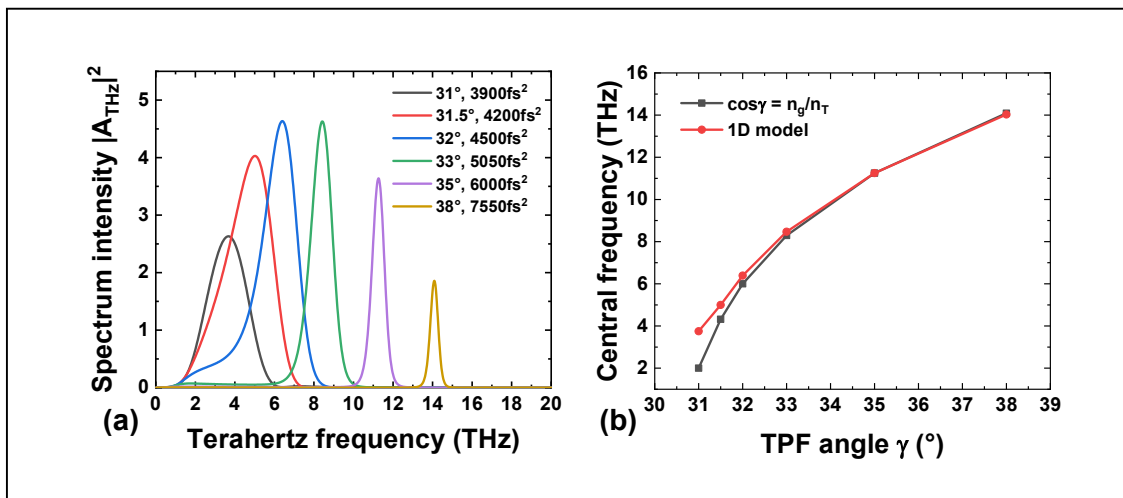


**Figure 4.** Spectrum tuning of TPF OR in 4H-SiC. (a) Terahertz spectrum intensity  $|A_{\text{THz}}|^2$  at six TPF angles under optimal GDD when  $L=4$  mm. (b) Shift of peak frequency versus TPF angle. The black dotted line is calculated by the PM condition  $\cos\gamma=n_g/n_T$ , while the red dotted line is simulated by the 1D model.

The evolution of terahertz spectrums versus  $L$  at different TPF angles are shown in Figure 5. Consistent with the previous analysis, lower frequency corresponds to more remarkable terahertz spectral splitting, widening and absorption due to the frequency-dependent PM allowance and

FCA effect. Less GDD aggravates the absorption, resulting in more efficiency decline and spectrum deterioration after reaching the maximum efficiency. It can be observed that there is similar oscillation and attenuation in efficiency to Figure 2. The oscillation period and amplitude depend on the PM bandwidth, reflecting the speed and strength of spectrum splitting and widening, while the efficiency attenuation mainly originates from FCA. Specially, obvious attenuation rather than oscillation appears at the low-frequency part due to serious absorption (TPF angle  $\leq 33^\circ$ ). As to the high-frequency part (TPF angle  $\geq 33^\circ$ ), there is neither obvious oscillation nor efficiency attenuation due to small PM bandwidth and absorptions. The simulation results also accord Figure 3 very well. With the increase of  $L$ , it fails to produce terahertz spectrum effectively under excessive pre-chirping, and reaches the optimal condition at  $L=4$  mm. Finally, spectrum splitting, widening and attenuation under insufficient pre-chirping appear, especially for the low-frequency part at small TPF angle.

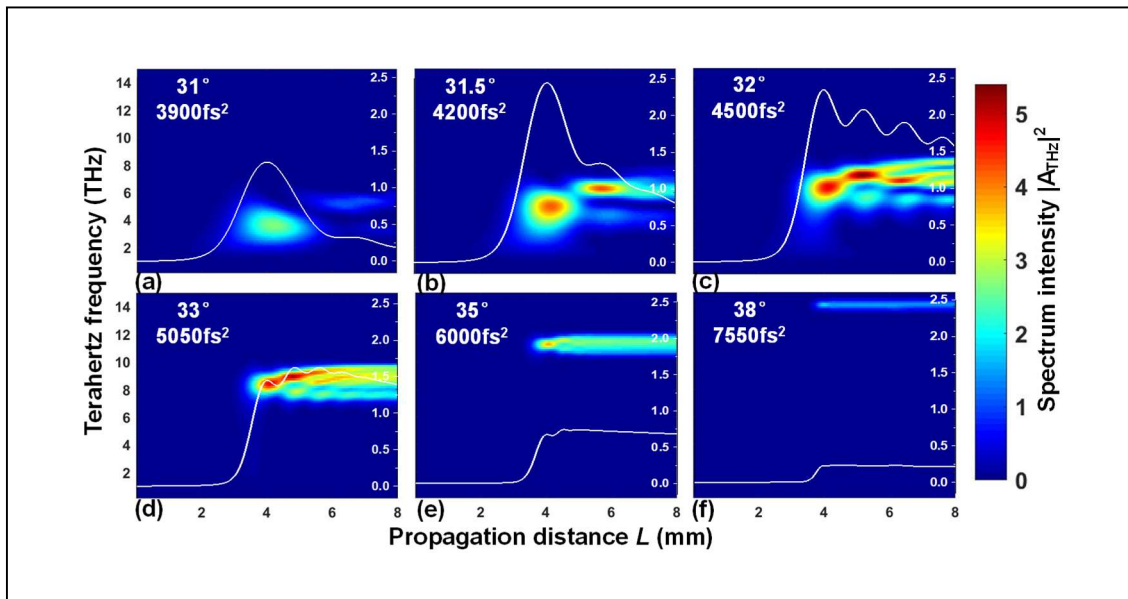


**Figure 5.** The evolution of terahertz spectrum intensity  $|A_{\text{THz}}|^2$  (color scale) along the propagation distance  $L$  at six TPF angles, under optimal GDD and at  $L=4$  mm. The white curve indicates the conversion efficiency as a function of  $L$ .

For a better understanding on the evolution of terahertz radiation with  $L$  under pre-chirping, the terahertz spectrum and temporal waveform at two different conditions are analyzed, as shown in Figure 6. The first case,  $\gamma=31.5^\circ$  and  $GDD=4200 \text{ fs}^2$ , and the results are given in Figure 6(a) and 6(b). When  $L$  is short (e.g., 1.5 mm), only low frequencies centered at 1.6 THz are generated and the spectral intensity is very low due to excessive pre-chirping, corresponding to a single-cycle terahertz pulse with the electric field amplitude of  $\sim 0.1 \text{ MV/cm}$ . As the interaction continues in a longer crystal, the terahertz pulse grows stronger and transforms into multi-cycle. The subsequent denser cycles are amplified faster, corresponding to the shift of peak frequency towards the higher frequency range (desired terahertz frequency at  $\gamma=31.5^\circ$ ) and increase the spectrum intensity gradually. When  $L=4 \text{ mm}$ , the electric field amplitude of the multi-cycle pulse reached  $\sim 1 \text{ MV/cm}$  with intensity-concentrated spectrum. If  $L$  is further increased to beyond the optimal value (e.g., 5.8 mm, the next oscillation peak in Figure 5), both the spectrum and temporal waveform are split and widened because of insufficient pre-chirping, as well as more absorption to lower frequencies. We can notice that there is only one continuous terahertz pulse throughout the crystal. However, the evolution of high-frequency terahertz waves includes two independent temporal pulses in the crystal, which is the second case. Taking  $\gamma=33^\circ$  and  $GDD=5050 \text{ fs}^2$  for example, the results are shown in Figure 6(c) and 6(d). Similar to the previous discussion, when the pre-chirped pulse just enters the crystal, the terahertz pulse was single-cycle and only low frequencies were produced. With longer propagation distance (e.g., 2.87 mm), periodical oscillation starts to appear after the initial single-cycle pulse, forming the other temporal pulse shown in Figure 6(d). The second pulse mainly contributes to the high-frequency range and greatly widens the spectral width together with the initial one, although the spectral intensity is still low. When  $L$  reaches the optimal value of 4

mm, we can observe the initial terahertz pulse and a clear amplified multi-cycle pulse in the temporal waveform. It proves that the generation and evolution of these two terahertz pulses are independent to each other. If  $L$  exceeds the optimal value (e.g., 4.85 mm, the next oscillation peak in Figure 5), both the terahertz spectrum and temporal waveform become split and widened, similar to the first case.

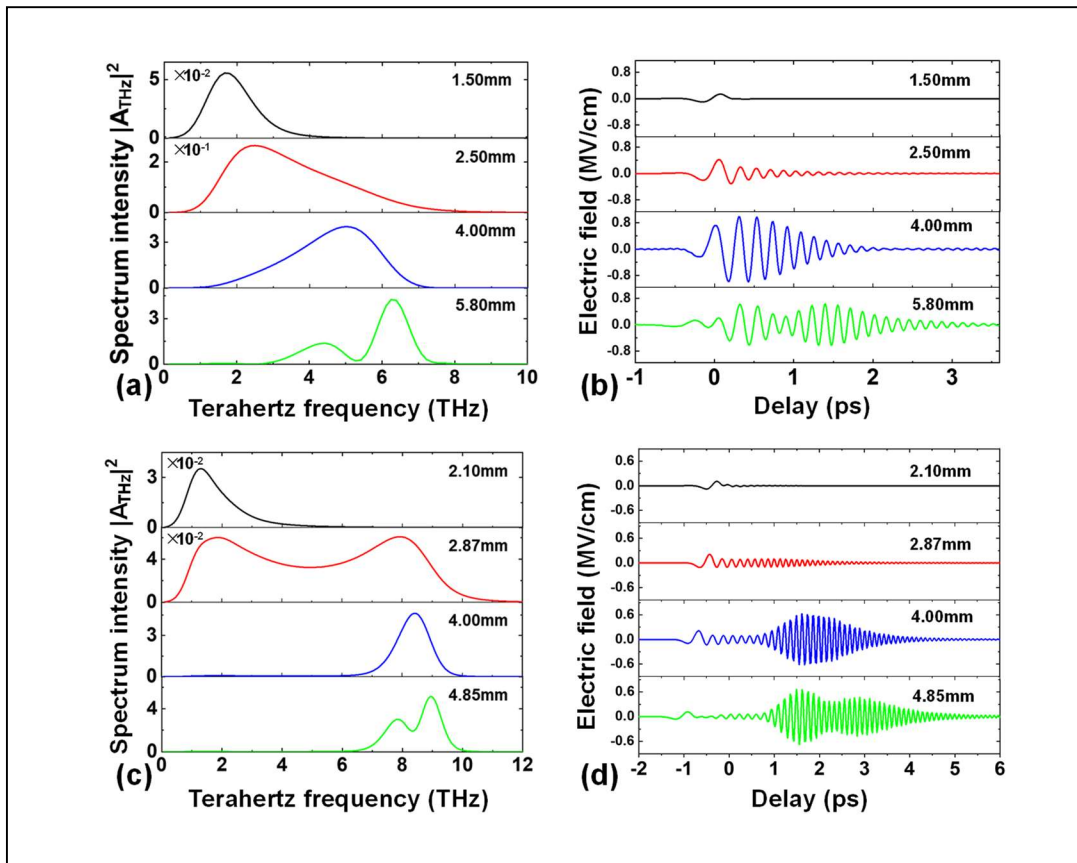


**Figure 6.** The evolution of terahertz spectrum ((a) and (c)) and temporal waveform ((b) and (d)) with  $L$  at two different conditions. (a) and (b):  $\gamma=31.5^\circ$ ,  $\text{GDD}=4200 \text{ fs}^2$ ; (c) and (d):  $\gamma=33^\circ$  and  $\text{GDD}=5050 \text{ fs}^2$ . The former forms only one continuous terahertz pulse throughout the crystal, while the latter forms two independent pulses.

Based on the above analysis, a scheme to modulate terahertz generation by pre-chirping can be proposed. Given  $\gamma=32^\circ$  and  $L=4$  mm, the terahertz spectrums and temporal waveforms with different GDDs are shown in Figure 7. The optimal GDD of  $4500 \text{ fs}^2$  corresponds to efficient, smooth and concentrated terahertz spectrum with strong multi-cycle electric-field amplitude up to  $\sim 0.8 \text{ MV/cm}$ . Tuning the GDD to  $7000 \text{ fs}^2$  leads to the generation of a near single-cycle terahertz pulse ( $\sim 0.2 \text{ MV/cm}$ ) with narrow spectrum centering at  $1.4 \text{ THz}$ . If the GDD is varied to  $6000 \text{ fs}^2$ , flat-top broadband terahertz spectrum ( $1\text{-}7.5 \text{ THz}$ , FWHM) can be obtained with considerable high intensity. Note that the bandwidth can be even wider under a larger TPF angle, but the spectral intensity and flatness will be degraded, similar to the above situation of  $\gamma=33^\circ$ . When the GDD is reduced to  $3500 \text{ fs}^2$ , it turns into split and widened terahertz spectrum and temporal waveform, in which the low-frequency part suffer attenuation due to the FCA effect.

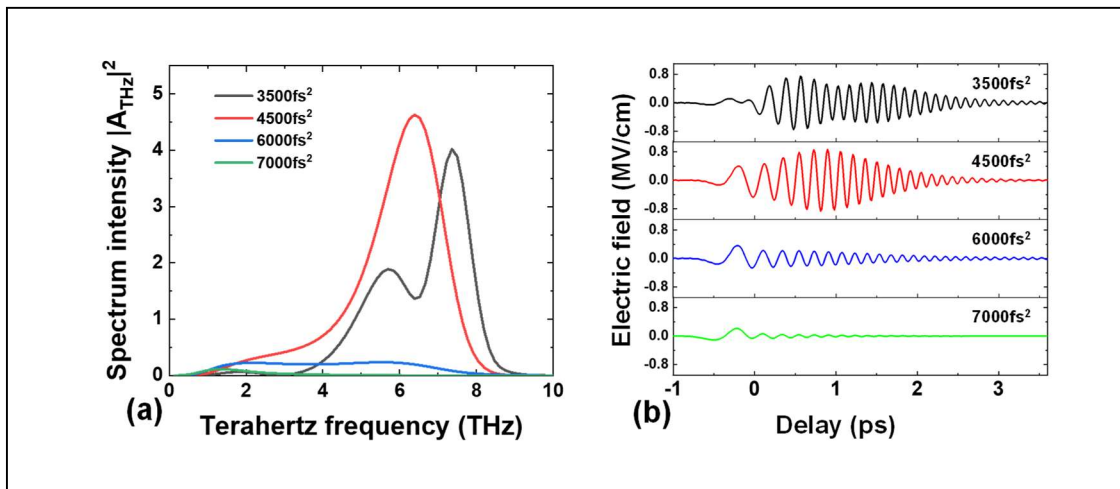


**Figure 7.** Modulation of terahertz spectrum (a) and temporal waveform (b) by varying pre-chirping when  $\gamma=32^\circ$  and  $L=4$  mm. Different terahertz spectrums (flat-top broadband, efficient and concentrated, splitted and widened) and temporal waveforms (single- to multi-cycle pulse) can be flexibly tuned by varying the GDD.

Generally, generating high-frequency terahertz waves by TPF OR in 4H-SiC is always accompanied by more and narrower temporal cycles with suitable GDD, which is demonstrated in Figure 6. Since the central frequency is tunable by the TPF angle, two typical cases,  $\gamma=31^\circ$  and  $\gamma=38^\circ$ , are discussed and the simulation results are shown in Figure 8. The GDDs are  $800 \text{ fs}^2$ ,  $4000 \text{ fs}^2$  and  $8000 \text{ fs}^2$  for both cases, while the optimal  $L$  are 0.62 mm, 4.12 mm and 8 mm for  $\gamma=31^\circ$ , and 0.445mm, 2.1mm and 4.19 mm for  $\gamma=38^\circ$ , respectively. Larger GDD with longer  $L$  excites more pulse cycles and longer pulse duration, corresponding to narrower and more concentrated terahertz spectrum. The blue shift of terahertz spectrum and low-frequency attenuation in Figure 8(a) are caused by strong FCA effect with low pre-chirping, while FCA exhibits little influence in Figure 8(c) because the high-frequency absorption by photocarriers is relatively weak. It is double confirmed here that higher frequency corresponds to narrower temporal cycle, where the cycle intervals for  $\gamma=31^\circ$  and  $\gamma=38^\circ$  are around 200 fs and 70 fs, respectively. The generation of multi-cycle terahertz pulse can be explained by the fact that the pump pulse is intensity-resonant, modulated by the initial pre-chirping and self-produced terahertz fields, which in turn produce multi-cycle terahertz waves efficiently during the interaction<sup>[47]</sup>. According to Figure 2, the maximum efficiency  $\eta_{\max}$  for  $\gamma=38^\circ$  stops increasing at  $L \approx 1 \text{ mm}$  so that the terahertz field amplitude would decrease to produce more pulse cycles and longer duration. It reveals the way of effective modulation on terahertz spectrum and waveform by pre-chirping (at optimal  $L$ ), i.e., even if the OR efficiency is saturated, narrower but more concentrated terahertz spectrum with the temporal waveform of more cycles is still achievable by increasing pre-chirping and  $L$ . The envelope fluctuation and enlarged interval between the initial pulse and the long multi-cycle pulse are observed with larger GDD and  $L$ , as shown in Figure 8(d). This phenomenon is also ascribed to the nonlinear optical interaction between the highly pre-chirped pump pulse and terahertz fields

through adequate propagation distance. Compared with the other methods for multi-cycle terahertz generation, e.g., OR in periodically-poled lithium niobate (PPLN)<sup>[70,71]</sup>, with intensity-modulated laser pulses<sup>[72,73]</sup>, and with chirped laser pulses<sup>[47]</sup>, the distinct advantages of TPF OR in 4H-SiC include ultra-wide tunable bandwidth and flexibility in manipulating the temporal waveform, which is of significant value in terahertz-driven X-ray sources<sup>[74,77]</sup>, compact accelerators<sup>[7,75-77]</sup>, resonant control over materials<sup>[3]</sup>, etc.

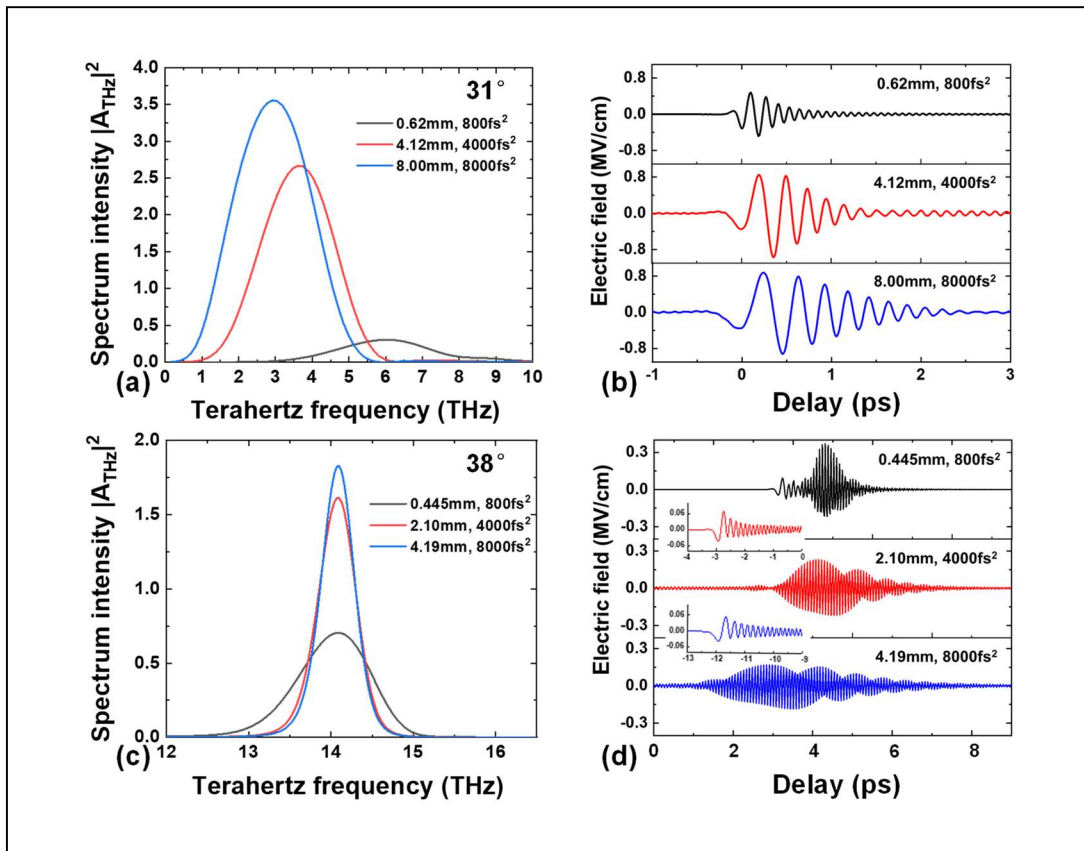


**Figure 8.** Terahertz spectrum ((a) and (c)) and temporal waveform ((b) and (d)) at different TPF angles ( $\gamma=31^\circ$  and  $\gamma=38^\circ$ ) and pre-chirping (GDD=800, 4000 and 8000 fs<sup>2</sup>) at the corresponding optimal  $L$ . The insets in (d) show the initially established terahertz signal when the pre-chirped pump pulse enters the crystal.

#### IV. CONCLUSION

Considering the excellent physical and optical properties of 4H-SiC, TPF OR based on this crystal was studied for the first time via the 1D model, accounting for coupled NLO interaction of the terahertz and optical waves, angular and material dispersions, linear absorption, FCA at terahertz frequency, SPM and pre-chirping of the pump pulse. Compared with LiNbO<sub>3</sub>, 4H-SiC-based TPF OR demonstrates great potential in producing ultra-widely tunable (up to over 14 THz) terahertz waves with high efficiency ( $\sim 10^{-2}$ ) and strong-field ( $\sim \text{MV/cm}$ ), while the TPF angle is only half of that in LiNbO<sub>3</sub>. The terahertz field can be further enhanced by focusing in experiments. Small TPF angle is a significant advantage to increase the effective interaction length and spatial uniformity, and reduce the GVD-AD and beam distortion, which greatly favors the contact grating (CG) design<sup>[21,42,49]</sup>. Pre-chirping the pump pulse was proved effective in modulating the terahertz spectrum and temporal pulse waveform. Flat-top broadband, efficient and concentrated, or splitted and widened spectrums are flexibly tunable by presetting the TPF angle, GDD and  $L$  properly. The corresponding terahertz pulse can be single-cycle or multi-cycle with the minimum interval of tens of femtoseconds. 4H-SiC-based TPF OR has extremely important potential in strong-field and ultra-wide bandwidth terahertz applications, including nonlinear terahertz spectroscopy, strong-field terahertz physics and electron acceleration, etc. In particular, multi-cycle terahertz pulse combines high acceleration gradient and long interaction distance, which is favorable for waveguide-based electron acceleration<sup>[75,76]</sup>. Multi-cycle narrowband terahertz pulse in the high-frequency range also provides a good solution for compact and efficient acceleration structures<sup>[77]</sup>. It should be noted that since 4H-SiC is a commercialized material in semiconductor industry, large size crystals are readily available benefitting from the mature growing and manufacturing technology, so that scaling the terahertz pulse energy is straightforward as long as the pump laser is powerful enough.



## Acknowledgement

This work was supported by the National Natural Science Foundation of China under Grant 62175184 and the Key Laboratory of Micro Opto-electro Mechanical System Technology, Ministry of Education.

## References

1. Hwang, H. Y., Fleischer, S., Brandt, N. C., Perkins, B. G., Liu, M., Fan, K., Sternbach, A., Zhang, X., Averitt, R. D., and Nelson, K. A., “A review of non-linear terahertz spectroscopy with ultrashort tabletop-laser pulses”, *J. Mod. Opt.* 62, 1447 (2015).
2. Elsaesser, T., Reimann, K., and Woerner, M., “Focus: Phase-resolved nonlinear terahertz spectroscopy-From charge dynamics in solids to molecular excitations in liquids”, *J. Chem. Phys.* 142, 212301 (2015).
3. Kampfrath, T., Tanaka, K., and Nelson, K. A., “Resonant and nonresonant control over matter and light by intense terahertz transients”, *Nat. Photon.* 7, 680 (2013).
4. Kampfrath, T., Sell, A., Klatt, G., Pashkin, A., Mährlein, S., Dekorsy, T., Wolf, M., Fiebig, M., Leitenstorfer, A., and Huber, R., “Coherent terahertz control of antiferromagnetic spin waves”, *Nat. Photon.* 5, 31 (2011).
5. Schubert, O., Hohenleutner, M., Langer, F., Urbanek, B., Lange, C., Huttner, U., Golde, D., Meier, T., Kira, M., Koch, S. W., and Huber, R., “Sub-cycle control of terahertz high-harmonic generation by dynamical Bloch oscillations”, *Nat. Photon.* 8, 119 (2014).
6. Takeda, J., Yoshioka, K., Minami, Y., and Katayama, I., “Nanoscale electron manipulation in metals with intense THz electric fields”, *J. Phys. D: Appl. Phys.* 51, 103001 (2018).
7. Liu, W., Sun, L., Yu, Z., Liu, Y., Jia, Q., Sun, B., and Xu, H., “THz-driven dielectric particle accelerator on chip”, *Opt. Lett.* 46, 4398 (2021).
8. Daranciang, D., Goodfellow, J., Fuchs, M., Wen, H., Ghimire, S., Reis, D. A., Loos, H., Fisher, A. S., and Lindenberg, A. M., “Single-cycle terahertz pulses with  $> 0.2$  V/Å field amplitudes via coherent transition radiation”, *Appl. Phys. Lett.* 99, 141117 (2011).

9. Li, H., Lu, Y., He, Z., Jia, Q., and Wang, L., “Generation of intense narrow-band tunable terahertz radiation from highly bunched electron pulse train”, *J. Infrared Milli. Terahz. Waves* 37, 649 (2016).
10. Kasai, S., Watanabe, M., and Ouchi, T., “Improved terahertz wave intensity in photoconductive antennas formed of annealed low-temperature grown GaAs”, *Jpn. J. Appl. Phys.* 46, 4163 (2007).
11. Ropagnol, X., Bouvier, M., Reid, M., and Ozaki, T., “Improvement in thermal barriers to intense terahertz generation from photoconductive antennas”, *J. Appl. Phys.* 116, 043107 (2014).
12. Xu, M., Mittendorff, M., Dietz, R. J. B., Künzel, H., Sartorius, B., Göbel, T., Schneider, H., Helm, M., and Winnerl, S., “Terahertz generation and detection with InGaAs-based large-area photoconductive devices excited at 1.55  $\mu\text{m}$ ”, *Appl. Phys. Lett.* 103, 251114 (2013).
13. Ropagnol, X., Khorasaninejad, M., Raeiszadeh, M., Safavi-Naeini, S., Bouvier, M., Côté, C. Y., Laramée, A., Reid, M., Gauthier, M. A., and Ozaki, T., “Intense THz Pulses with large ponderomotive potential generated from large aperture photoconductive antennas”, *Opt. Express* 24, 11299 (2016).
14. Seifert, T. S., Cheng, L., Wei, Z., Kampfrath, T., and Qi, J., “Spintronic sources of ultrashort terahertz electromagnetic pulses”, *Appl. Phys. Lett.* 120, 180401 (2022).
15. Rouzegar, R., Chekhov, A. L., Behovits, Y., Serrano, B. R., Syskaki, M. A., Lambert, C. H., Engel, D., Martens, U., Münzenberg, M., Wolf, M., Jakob, G., Kläui, M., Seifert, T. S., and Kampfrath, T., “Broadband Spintronic Terahertz Source with Peak Electric Fields Exceeding 1.5 MV/cm”, *Phys. Rev. Appl.* 19, 034018 (2023).
16. Hamster, H., Sullivan, A., Gordon, S., White, W., and Falcone, R. W., “Subpicosecond, electromagnetic pulses from intense laser-plasma interaction”, *Phys. Rev. Lett.* 71, 2725 (1993).
17. Koulouklidis, A. D., Gollner, C., Shumakova, V., Fedorov, V. Y., Pugžlys, A., Baltuška, A., and Tzortzakis, S., “Observation of extremely efficient terahertz generation from mid-infrared two-color laser filaments”, *Nat. Commun.* 11, 292 (2020).
18. Hauri, C. P., Ruchert, C., Vicario, C., and Ardana, F., “Strong-field single-cycle THz pulses generated in an organic crystal”, *Appl. Phys. Lett.* 99, 161116 (2011).

19. Roeder, F., Shalaby, M., Beleites, B., Ronneberger, F., and Gopal, A., “THz generation by optical rectification of intense near-infrared pulses in organic crystal BNA”, *Opt. Express* 28, 36274 (2020).
20. Zhang, B., Ma, Z., Ma, J., Wu, X., Ouyang, C., Kong, D., Hong, T., Wang, X., Yang, P., Chen, L., Li, Y., and Zhang, J., “1.4-mJ high energy terahertz radiation from lithium niobates”, *Laser Photonics Rev.* 15, 2000295 (2021).
21. Polónyi, Gy., Monoszlai, B., Andriukaitis, G., Gäumann, G., Balciunas, T., Pugzlys, A., Baltuska, A., Feurer, T., Hebling, J., and Fülöp, J. A., “High-energy terahertz pulses from semiconductors pumped beyond the three photon absorption edge”, *Opt. Express* 24, 23872 (2016).
22. Zhang, Y., Li, K., and Zhao, H., “Intense terahertz radiation: generation and application”, *Front. Optoelectron.* 14, 4 (2021).
23. Blanchard, F., Razzari, L., Bandulet, H. C., Sharma, G., Morandotti, R., Kieffer, J. C., Ozaki, T., Reid, M., Tiedje, H. F., Haugen, H. K., and Hegmann, F. A., “Generation of 1.5  $\mu$ J single-cycle terahertz pulses by optical rectification from a large aperture ZnTe crystal”, *Opt. Express* 15, 13212 (2007).
24. Löffler, T., Hahn, T., Thomson, M., Jacob, F., and Roskos, H. G., “Large-area electro-optic ZnTe terahertz emitters”, *Opt. Express* 13, 5353 (2005).
25. Hekmat, N., Vogel, T., Wang, Y., Mansourzadeh, S., Aslani, F., Omar, A., Hoffmann, M., Meyer, F., and Saraceno, C. J., “Cryogenically cooled GaP for optical rectification at high excitation average powers”, *Opt. Mater. Express* 10, 2768 (2020).
26. Ji, W., Kukaswadia, A. K., Feng, Z. C., Tang, S. H., and Becla, P., “Nonlinear refraction and optical limiting in bulk ZnTe crystal”, *J. Cryst. Growth* 138, 187 (1994).
27. L. P. Gonzalez, S. Guha, and S. Trivedi, “Damage thresholds and nonlinear optical performance of GaP”, in *Conference on Lasers and Electro-Optics* (San Francisco, CA, USA, 2004), p. CWA47.
28. Meng, Q., Zhang, B., Zhong, S., and Zhu, L., “Damage threshold of lithium niobate crystal under single and multiple femtosecond laser pulses: theoretical and experimental study”, *Appl. Phys. A* 122, 582 (2016).

29. Moriguchi, Y., Tokizane, Y., Takida, Y., Nawata, K., Eno, T., Nagano, S., and Minamide, H., “High-average and high-peak output-power terahertz-wave generation by optical parametric down-conversion in MgO:LiNbO<sub>3</sub>”, *Appl. Phys. Lett.* 113, 121103 (2018).
30. Wang, W., Zhang, X., Wang, Q., Cong, Z., Chen, X., Liu, Z., Qin, Z., Li, P., Tang, G., Li, N., Wang, C., Li, Y., and Cheng, W., “Multiple-beam output of a surface-emitted terahertz-wave parametric oscillator by using a slab MgO:LiNbO<sub>3</sub> crystal”, *Opt. Lett.* 39, 754 (2014).
31. Wang, Y., Tang, L., Xu, D., Yan, C., He, Y., Shi, J., Yan, D., Liu, H., Nie, M., Feng, J., and Yao, J., “Energy scaling and extended tunability of terahertz wave parametric oscillator with MgO-doped near-stoichiometric LiNbO<sub>3</sub> crystal”, *Opt. Express* 25, 8926 (2017).
32. Hebling, J., Almási, G., Kozma, I., and Kuhl, J., “Velocity matching by pulse front tilting for large area THz-pulse generation”, *Opt. Express* 10, 1161 (2002).
33. Fülöp, J. A., Pálfalvi, L., Klingebiel, S., Almási, G., Krausz, F., Karsch, S., and Hebling, J., “Generation of sub-mJ terahertz pulses by optical rectification”, *Opt. Lett.* 37, 557 (2012).
34. Fülöp, J. A., Ollmann, Z., Lombosi, Cs., Skrobol, C., Klingebiel, S., Pálfalvi, L., Krausz, F., Karsch, S., and Hebling, J., “Efficient generation of THz pulses with 0.4mJ energy”, *Opt. Express* 22, 20155 (2014).
35. Wu, X., Chai, S., Ma, J., Zhang, B., Xia, C., Fang, Z., Kong, D., Wang, J., Liu, H., Zhu, C., Wang, X., Ruan, C., and Li, Y., “Optimization of highly efficient terahertz generation in lithium niobate driven by Ti:sapphire laser pulses with 30 fs pulse duration”, *Chin. Opt. Lett.* 16, 041901 (2018).
36. Wu, X., Ma, J., Zhang, B., Chai, S., Fang, Z., Xia, C., Kong, D., Wang, J., Liu, H., Zhu, C., Wang, X., Ruan, C., and Li, Y., “Highly efficient generation of 0.2 mJ terahertz pulses in lithium niobate at room temperature with sub-50 fs chirped Ti:sapphire laser pulses”, *Opt. Express* 26, 7107 (2018).
37. Lombosi, Cs., Polónyi, Gy., Mechler, M., Ollmann, Z., Hebling, J., and Fülöp, J. A., “Nonlinear distortion of intense THz beams”, *New J. Phys.* 17, 083041 (2015).
38. Fülöp, J. A., Pálfalvi, L., Almási, G., and Hebling, J., “Design of high-energy terahertz sources based on optical rectification”, *Opt. Express* 18, 12311 (2010).
39. Fülöp, J. A., Pálfalvi, L., Hoffmann, M. C., and Hebling, J., “Towards generation of mJ-level ultrashort THz pulses by optical rectification”, *Opt. Express* 19, 15090 (2011).

40. Bodrov, S. B., Murzanev, A. A., Sergeev, Y. A., Malkov, Y. A., and Stepanov, A. N., “Terahertz generation by tilted-front laser pulses in weakly and strongly nonlinear regimes”, *Appl. Phys. Lett.* 103, 251103 (2013).
41. Bakunov, M. I., Bodrov, S. B., and Mashkovich, E. A., “Terahertz generation with titled-front laser pulses: dynamic theory for low absorbing crystals”, *J. Opt. Soc. Am. B* 28, 1724 (2011).
42. Bakunov, M. I. and Bodrov, S. B., “Terahertz generation with tilted-front laser pulses in a contact-grating scheme”, *J. Opt. Soc. Am. B* 31, 2549 (2014).
43. Ravi, K., Huang, W. R., Carbajo, S., Wu, X., and Kärtner, F. X., “Limitations to THz generation by optical rectification using tilted pulse fronts”, *Opt. Express* 22, 20239 (2014).
44. Ravi, K., Huang, W. R., Carbajo, S., Nanni, E. A., Schimpf, D. N., Ippen, E. P., and Kärtner, F. X., “Theory of terahertz generation by optical rectification using tilted-pulse-fronts”, *Opt. Express* 23, 5253 (2015).
45. Tóth, G., Pálfalvi, L., Fülöp, J. A., Krizsán, G., Matlis, N. H., Almási, G., and Hebling, J., “Numerical investigation of imaging-free terahertz generation setup using segmented tilted-pulse-front excitation”, *Opt. Express* 27, 7762 (2019).
46. Wang, L., Kroh, T., Matlis, N. H., and Kärtner, F. X., “Full 3D+1 modelling of the tilted-pulse-front setups for single-cycle terahertz generation”, *J. Opt. Soc. Am. B* 37, 1000 (2020).
47. Jang, D. and Kim, K. Y., “Multicycle terahertz pulse generation by optical rectification in LiNbO<sub>3</sub>, LiTaO<sub>3</sub>, and BBO crystals”, *Opt. Express* 28, 21220 (2020).
48. Wang, L., Tóth, G., Hebling, J., and Kärtner, F. X., “Tilted-pulse-front schemes for terahertz generation”, *Laser Photonics Rev.* 14, 2000021 (2020).
49. Ollmann, Z., Fülöp, J. A., Hebling, J., and Almási, G., “Design of a high-energy terahertz pulse source based on ZnTe contact grating”, *Opt. Commun.* 315, 159 (2014).
50. Blanchard, F., Schmidt, B. E., Ropagnol, X., Thiré, N., Ozaki, T., Morandotti, R., Cooke, D. G., and Légaré, F., “Terahertz pulse generation from bulk GaAs by a tilted-pulse-front excitation at 1.8 $\mu$ m”, *Appl. Phys. Lett.* 105, 241106 (2014).
51. Pálfalvi, L., Hebling, J., Kuhl, J., Péter, Á., and Polgár, K., “Temperature dependence of the absorption and refraction of Mg-doped congruent and stoichiometric LiNbO<sub>3</sub> in the THz range”, *J. Appl. Phys.* 97, 123505 (2005).

52. Wu, X., Zhou, C., Huang, W. R., Ahr, F., and Kärtner, F. X., “Temperature dependent refractive index and absorption coefficient of congruent lithium niobate crystals in the terahertz range”, *Opt. Express* 23, 29729 (2015).
53. Niedermeier, S., Schillinger, H., Sauerbrey, R., Adolph, B., and Bechstedt, F., “Second-harmonic generation in silicon carbide polytypes”, *Appl. Phys. Lett.* 75, 618 (1999).
54. K. Nakayama, A. Matsubara, S. Okajima, K. Kawahata, K. Tanaka, T. Akiyama, H. Kinoshita, M. Yoshimoto, and T. Takahashi, “Precise measurements of optical constants of SiC in 40 to 120  $\mu\text{m}$  wavelength region,” in *35th International Conference on Infrared, Millimeter, and Terahertz Waves* (Rome, Italy, 2010), p. 1.
55. Wang, S., Zhan, M., Wang, G., Xuan, H., Zhang, W., Liu, C., Xu, C., Liu, Y., Wei, Z., and Chen, X., “4H-SiC a new nonlinear material for midinfrared lasers”, *Laser Photonics Rev.* 7, 831 (2013).
56. Fan, H., Xu, C., Wang, Z., Wang, G., Liu, C., Liang, J., Chen, X., and Wei, Z., “Generation of broadband 17- $\mu\text{J}$  mid-infrared femtosecond pulses at 3.75  $\mu\text{m}$  by silicon carbide crystal”, *Opt. Lett.* 39, 6249 (2014).
57. Naftaly, M., Molloy, J. F., Magnusson, B., Andreev, Y. M., and Lanskii, G. V., “Silicon carbide—a high-transparency nonlinear material for THz applications”, *Opt. Express* 24, 2590 (2016).
58. Fischer, M. P., Bühler, J., Fitzky, G., Kurihara, T., Eggert, S., Leitenstorfer, A., and Brida, D., “Coherent field transients below 15 THz from phase-matched difference frequency generation in 4H-SiC”, *Opt. Lett.* 42, 2687 (2017).
59. G. L. Harris, *Properties of Silicon Carbide* (INSPEC, DC, USA, 1995).
60. Strait, J. H., George, P. A., Dawlaty, J., Shivaraman, S., Chandrashekhara, M., Rana, F., and Spencer, M. G., “Emission of terahertz radiation from SiC”, *Appl. Phys. Lett.* 95, 051912 (2009).
61. Guo, X., Peng, Z., Ding, P., Li, L., Chen, X., Wei, H., Tong, Z., and Guo, L., “Nonlinear optical properties of 6H-SiC and 4H-SiC in an extensive spectral range”, *Opt. Mater. Express* 11, 1080 (2021).
62. Nagai, M., Matsubara, E., and Ashida, M., “High-efficiency terahertz pulse generation via optical rectification by suppressing stimulated Raman scattering process”, *Opt. Express* 20, 6509 (2012).

63. Apostolopoulos, V. and Barnes, M. E., “THz emitters based on the photo-Dember effect”, *J. Phys. D: Appl. Phys.* 47, 374002 (2014).
64. Wu, H., Guo, Q., Tu, Y., Lyu, Z., Wang, X., Li, Y., Zhou, Z., Zhang, D., Zhao Z., and Yuan, J., “Polarity Reversal of Terahertz Electric Field from Heavily p-Doped Silicon Surfaces”, *Chin. Phys. Lett.* 38, 074201 (2021).
65. Zhong, S., Zhai, Z., Li, J., Zhu, L., Li, J., Meng, K., Liu, Q., Du, L., Zhao, J., and Li, Z., “Optimization of terahertz generation from LiNbO<sub>3</sub> under intense laser excitation with the effect of three-photon absorption”, *Opt. Express* 23, 31313 (2015).
66. Grivickas, V., Galeckas, A., Grivickas, P., and Linnros, J., “Determination of the polarization dependence of the free-carrier-absorption in 4H-SiC at high-level photoinjection”, *Mater. Sci. Forum* 338–342, 555 (2000).
67. Gu, B., He, J., Ji, W., and Wang, H., “Three-photon absorption saturation in ZnO and ZnS crystals”, *J. Appl. Phys.* 103, 073105 (2008).
68. P. E. Powers and J. W. Haus, *Fundamentals of Nonlinear Optics, 2nd ed.* (CRC, Boca Raton, FL, USA, 2011).
69. Sato, H., Abe, M., Shoji, I., Suda, J., and Kondo, T., “Accurate measurements of second-order nonlinear optical coefficients of 6H and 4H silicon carbide”, *J. Opt. Soc. Am. B* 26, 1892 (2009).
70. L’huillier, J. A., Torosyan, G., Theuer, M., Avetisyan, Y., and Beigang, R., “Generation of THz radiation using bulk, periodically and aperiodically poled lithium niobate– Part 1: Theory”, *Appl. Phys. B* 86, 185 (2007).
71. Carbajo, S., Schulte, J., Wu, X., Ravi, K., Schimpf, D. N., and Kärtner, F. X., “Efficient narrowband terahertz generation in cryogenically cooled periodically poled lithium niobate”, *Opt. Lett.* 40, 5762 (2015).
72. Tóth, G., Fülöp, J., and Hebling, J., “Periodically intensity-modulated pulses by optical parametric amplification for multicycle tunable terahertz pulse generation”, *Opt. Express* 25, 28258 (2017).
73. Nugraha, P. S., Krizsán, G., Polónyi, Gy., Mechler, M. I., Hebling, J., Tóth, Gy., and Fülöp, J. A., “Efficient semiconductor multicycle terahertz pulse source”, *J. Phys. B: At. Mol. Opt. Phys.* 51, 094007 (2018).

74. Kärtner, F. X., Ahr, F., Calendron, A. -L., Çankaya, H., Carbajo, S., Chang, G., Cirmi, G., Dörner, K., Dorda, U., Fallahi, A., Hartin, A., Hemmer, M., Hobbs, R., Hua, Y., Huang, W. R., Letrun, R., Matlis, N., Mazalova, V., Mücke, O. D., Nanni, E., Putnam, W., Ravi, K., Reichert, F., Sarrou, I., Wu, X., Yahaghi, A., Ye, H., Zapata, L., Zhang, D., Zhou, C., Miller, R. J. D., Berggren, K. K., Graafsma, H., Meents, A., Assmann, R. W., Chapman, H. N., and Fromme, P., “AXSIS: Exploring the frontiers in attosecond X-ray science, imaging and spectroscopy”, *Nucl. Instrum. Methods. Phys. Res. A* 829, 24 (2016).
75. Wong, L. J., Fallahi, A., and Kärtner, F. X., “Compact electron acceleration and bunch compression in THz waveguides”, *Opt. Express* 21, 9792 (2013).
76. Zhang, D., Zeng, Y., Fakhari, M., He, X., Matlis, N. H., and Kärtner, F. X., “Long range terahertz driven electron acceleration using phase shifters”, *Appl. Phys. Rev.* 9, 031407 (2022).
77. Matlis, N. H., Ahr, F., Calendron, A. -L., Cankaya, H., Cirmi, G., Eichner, T., Fallahi, A., Fakhari, M., Hartin, A., Hemmer, M., Huang, W. R., Ishizuki, H., Jolly, S. W., Leroux, V., Maier, A. R., Meier, J., Qiao, W., Ravi, K., Schimpf, D. N., Taira, T., Wu, X., Zapata, L., Zapata, C., Zhang, D., Zhou, C., and Kärtner, F. X., “Acceleration of electrons in THz driven structures for AXSIS”, *Nucl. Instrum. Methods. Phys. Res. A* 909, 27 (2018).